Results in Materials 22 (2024) 100583

Contents lists available at ScienceDirect

Results in Materials

journal homepage: www.sciencedirect.com/journal/results-in-materials

The surface tension of boiling steel surfaces

Joerg Volpp [a,f,*], Yuji Sato [b], Masahiro Tsukamoto [b], Lewin Rathmann [c], Marius Möller [c], Samuel J. Clark [d], Kamel Fezzaa [d], Tim Radel [d], Kevin Klingbeil [e]

[a] Department of Engineering Sciences and Mathematics, Luleå University of Technology, 971 87, Luleå, Sweden
[b] Joining and Welding Research Institute (JWRI), Osaka University, 11-1 Mihogaoka, Ibaraki, Osaka, 567-0047, Japan
[c] BIAS - Bremer Institut für Angewandte Strahltechnik GmbH, Bremen, 28359, Germany
[d] X-ray Science Division, Advanced Photon Source, Argonne National Laboratory, Lemont, IL, 60439, USA
[e] Cross Product Solutions, LLC, Osceola, WI, 54020, USA
[f] Department of Mechanical Engineering, University West, Sweden

ARTICLE INFO

Keywords:
Keyhole walls
Pressure equilibrium
Recoil pressure
Laser beam

ABSTRACT

Material properties of metals and metal alloys at high temperatures are often unknown, but necessary to understand physical mechanisms for prediction and improvement of high temperature processes, such as laser beam technologies. Surface tension is an elementary property that was measured in this study above the boiling temperature of steel using a laser-induced vapor channel in a steel substrate and the extraction of the vapor channel diameter from in-situ X-ray observations. The measurement principle is based on the pressure balance inside the keyhole, where the recoil pressure from keyhole wall vaporization works against the surface tension pressure from the surrounding melt pool. An increase in surface tension at increasing temperatures above the boiling point was measured against theoretical expectations. In order to create the keyhole shapes measured, the surface tension must increase to counterbalance the increasing recoil pressure.

1. Introduction

Surface tension is an elementary property of materials. For metals, the values are often not available, in particular not at high temperatures close or even above boiling temperatures. However, to understand material behavior and to have reliable input for material and process simulations, surface tension data is highly relevant. Many high-temperature processes include surface tension effects, such as casting, laser beam, electron beam or plasma processing (welding, cutting, Additive Manufacturing, etc.). Surface tension often defines the quality of the process results. Therefore, it is highly desired to know and understand the surface tension of metals at high temperatures.

Surface tension is a mechanical force on the surface area parallel to a liquid surface due to attractive forces between atoms or molecules [1]. Surface tension can be basically understood in two ways. First, it can be seen as the amount of energy that is required to integrate molecules or atoms from the bulk material into its surface to enlarge it (energy per area, unit: J/m^2) [2]. Second, the surface tension can be understood as the resistance to a force to lengthen a liquid surface (force per length, unit N/m).

Surface tension is related to the heat of vaporization at absolute zero and the impact of the atomic neighbors [2]. Since also the kinetic energy change of electrons needs to be considered, liquid metals show lower surface tension values than expected from calculations [2]. At increasing temperature, the surface tension decreases for most pure materials [3]. For iron, surface tension data is available up to ~2500 K (e.g. Ref. [4]). Typically, a linear decrease is assumed based on measurements just above melting temperatures (e.g. Ref. [3]). E.g. Morohoshi et al. [5] measured the surface tension of iron σ_{Fe} in highly pure Argon atmosphere and derived the temperature T dependent linear equation

$$\sigma_{Fe} = (1925 \pm 65)\frac{N}{m} - (0.455 \pm 0.034)\frac{N}{m \bullet K} \bullet (T - 1808K) \quad (1)$$

This decrease is explained by the increasing vibration and distance between the atoms and the reduced attractive forces. For steel containing different alloying elements, variations can occur, such as an increasing tendency of surface tension that was observed just above the melting temperature followed by a decrease, which was related to the occurring impurities in the alloy (e.g. Ref. [6]). At very high temperatures far above the melting temperature, only scarce data is available from experimental measurements and theoretical predictions are

* Corresponding author.
E-mail address: jorg.volpp@hv.se (J. Volpp).

https://doi.org/10.1016/j.rinma.2024.100583
Received 15 March 2024; Received in revised form 3 May 2024; Accepted 4 June 2024
Available online 5 June 2024

difficult. However, several effects happening at temperatures closer to boiling temperature are known to be non-linear with temperature (e.g. rate of vaporization or ionic bond strength). Since the physical conditions at an increasing temperature significantly change, a simple extrapolation from data points generated at lower temperatures seems not appropriate. A linear decrease would also suggest that the surface tension disappears at a certain temperature. However, this state was not observed even at boiling metal surfaces.

Therefore, this work investigated the surface tension at elevated temperatures to gain a better understanding of its temperature dependence and physical effects.

2. Theory

2.1. Surface tension

At increasing metal temperatures above the melting point, thermal expansion happens that increases the atom distance. Thermal expansion occurs, however, not due to increased atomic vibration amplitudes, but due to the asymmetric curvature of the potential energy trough (e.g. Ref. [7]). A larger distance between the ions should denote a lower surface tension, which is the main expectation in literature. However, at the same time, the Fermi band broadening can be suspected to play a counteracting role (e.g. Refs. [8,9]). This would mean that the ions increase their probability to have more conduction electrons, which in turn increases the ion charge and thereby the Coulomb forces (e.g. Ref. [10]). Those additional forces can lead to an increased surface tension. In addition, when extensive vaporization happens on the boiling surface, atoms are ejected from the surface [11] denoting holes in the surface, which should also affect the surface tension due to missing bonding forces to the previous neighbors within the surface. Those additional effects at high temperatures are scarcely explored due to practical reasons and many unclear impacts but are relevant to understand surface tension at such extreme conditions.

2.2. Surface tension measurement

In order to investigate impacts on surface tension, surface tension needs to be measured. Surface tension measurement methods can be categorized in 1) direct measurement using microbalance, 2) measurement of capillary pressure, 3) capillary-gravity force analysis, 4) gravity-distorted drops and 5) reinforced drop distortion [12]. For liquid metals, the maximum bubble pressure method can be used to measure the pressure peak while forming a gas bubble inside the liquid material, which relates to the surface tension of the liquid material. Using droplets (e.g. sessile drop method) wetting a surface of another material contains potential measurement errors since the interfacial tension is often not known and wetting depends also on surface roughness and material temperatures.

Therefore, for metals, non-contact methods are desired. Those contain e.g. levitated drops (e.g. Refs. [13,14]) or falling drops. Using drop-on-demand techniques to form an oscillating drop can give surface tension values based on the frequency pattern at temperatures around the melting point of metals (e.g. Ref. [15]). However, it remains difficult to measure surface tension at higher temperatures. For iron and steel, the maximum temperatures reached during reported surface tension measurements are typically up to ~2500 K (e.g. Refs. [16–18]).

In addition, characteristics of surface wave propagation on liquid metals offers the possibility to derive surface tension information (e.g. Ref. [19]). Those measurements do not require contact of a measuring device with the liquid, which opens the possibility to use this method also for high-temperature metal surfaces. At Bond numbers $Bo \ll 1$, capillary waves experience restoring forces from mainly surface tension. Therefore, the Kelvin relation (e.g. Ref. [20]) can be used to derive the surface tension based on the wave frequency, wavelength, and material density [21]. The Kelvin equation is not restricted to a certain temperature range [22]. Due to the complex interplay of fluid motion, gravity, pressure gradients and viscous forces in a metal melt pool, impacts on surface tension were evaluated. It was shown that the vapor recoil pressure on the material surface has no stabilizing or destabilizing effect on the melt pool surface waves [23]. The Marangoni flow can slightly decrease the surface wave frequencies [24].

It remains difficult to produce a surface with a homogeneous high temperature without influencing the surface tension measurement results due to the increasing evaporation rates, that can alter the measuring conditions [6]. Therefore, this work aims to derive high-temperature surface tension values using indirect measurement methods and reveal trends about surface tension effects at very high temperatures.

3. Methods

For measuring the surface tension at very high temperatures of liquid metals, environments are needed that provide conditions that induce high temperatures and give the possibility to observe relevant characteristics. The vapor channel, also called keyhole, which is induced in laser deep penetration processes, can be such an environment. Since the laser beam energy input creates the vapor channel, high keyhole wall temperatures are reached, while the keyhole dimensions are defined by the pressure equilibrium between the recoil pressure from the vaporizing surface against the surface tension pressure from the surrounding liquid (e.g. Ref. [25]). Since the surface tension is part of the system, the keyhole can be used to derive surface tension values.

3.1. X-ray analyses

Therefore, surface tension values were determined using X-ray keyhole observations. X-ray keyhole analyses were performed in two places, namely at the Argonne National Lab's Advanced Photon Source using the 32-ID-B beamline and at Osaka University (Fig. 1).

Micro-welding of 316 L stainless steel under inert Argon atmosphere was done in Argonne National Lab using inline high speed X-ray imaging. A SCANLAB IntelliScan 30-de scan head was used to produce a 200 µm beam diameter on the material surface, guiding 200 W laser output power at a processing speed of 200 mm/s. High-speed X-ray imaging was performed with a polychromatic X-ray beam with a first harmonic energy of ~24 keV and an energy bandwidth of ~7 % generated by a 1.8 cm short period undulator with a gap of 11.5 mm. The portion of X-ray beam that was transmitted through the sample was incident upon a 100 µm thick LuAG:Ce scintillator. The visible light emitted by the

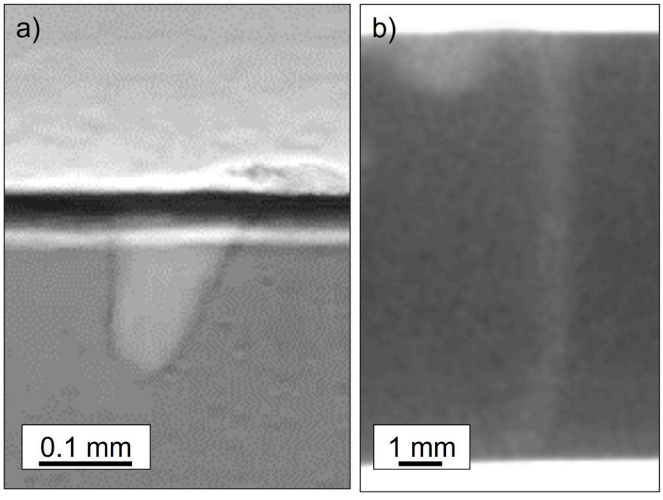

Fig. 1. Keyhole shape appearance examples in high-speed X-ray images of partial penetration welding at a) Argonne National Lab and b) Osaka university.

scintillator was recorded using a high-speed camera (Photron, FASTCAM SA-Z 2100K) at a 50 kHz frame rate and an exposure time of 19 µs. The window imaged was 2 mm in width and 0.5 mm in height. Keyhole frames at several times were extracted for evaluation of the surface tensions in the keyhole sections.

Thick steel plate welding was performed at Osaka university with inline X-ray radiography recording. The stainless-steel sheets were 8 mm and 14 mm thick, the laser beam had a spot diameter of 350 µm at a focal distance of 280 mm and was applied, while the material underneath was moved at a welding speed of 6 m/min on a weld seam length of 30 mm. Argon gas was applied. X-ray observation was performed at a viewing angle of 0° and a recording frequency of 1000 fps (FOD 130 mm; FID 550 mm). The X-ray tube current was 90 kV and the X-ray tube voltage 90 mA. The laser power was varied between 6 kW, 10 kW and 14 kW, while representative X-ray frames were taken for each case for the keyhole analysis.

3.2. Keyhole element analysis

Laser-induced vapor capillaries, or keyholes, were created while remelting steel surfaces. Keyhole dimensions were observed from the side using X-ray imaging (Fig. 2). The keyhole boundaries were detected using edge detection from a binarized picture (MATLAB). For the calculation of the energy input into the keyhole, the keyhole was split into ten sections in depth. Ten sections were found to provide sufficient accuracy [25]. The absorbed energy in each of the keyhole sections was determined by a combined vapor absorption and 2D-ray tracing algorithm [26]. A total of 20 rays was applied that represents the actual beam shape.

Every ray carried the integrated power of the circular beam of Gaussian-like shape through the related surface area, which is defined as the initial intensity. On the keyhole walls, Fresnel absorption was considered as absorption mechanism before the rays were reflected using geometrical optic laws. After all rays left the keyhole again, the energy in each element was taken as the energy input in all cylindrically assumed keyhole elements. Considering heat conduction losses, the temperatures of the keyhole sections were calculated. The temperatures were then used to calculate the pressure balance in each section [26,27]. Assuming that the ablation pressure p_{abl} is mainly balanced by the surface tension pressure p_{ST} ($p_{abl} = p_{ST}$) in the pressure balance equation (e.g. Ref. [27]), two main variables occur, namely the diameter of the keyhole section r and the surface tension σ.

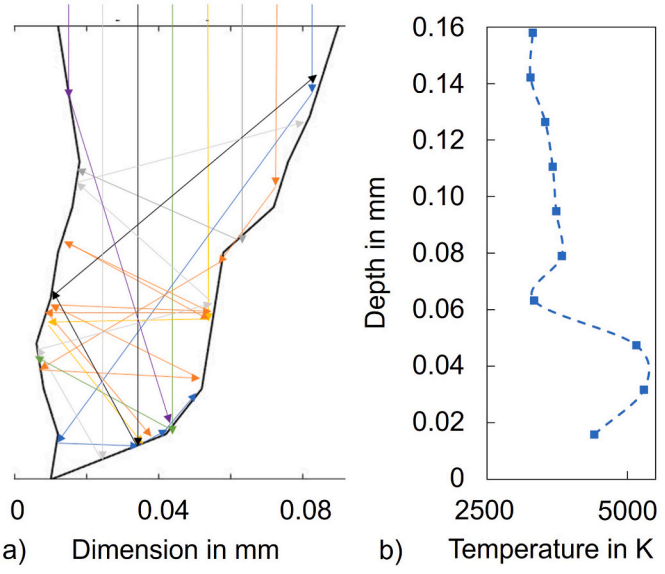

Fig. 2. a) 2-D keyhole reproduction from an X-ray image and example of ray propagations within the keyhole; b) resulting temperature distribution after multiple reflections and absorption.

$$\frac{I_v}{L_v} \bullet \left(\frac{\kappa \bullet R \bullet T_s}{M} \right) = \frac{\sigma}{r} \tag{2}$$

Those depend on the intensity used for vaporization I_v, the latent heat of vaporization L_v (10 800 kJ/kg), the thermal diffusivity κ (40e-6), the molar gas constant R and the molar mass M (24.3 g/mol). Since the keyhole diameters were derived from the X-ray frames of the stable keyhole sections, the related surface tension was calculated in each keyhole section in depth.

The error of measuring the keyhole diameters lead to uncertainties of the surface tension measurements. Type B uncertainties were estimated. Based on the symmetrically assumed deviation Δ, the uncertainties u_B were derived for each surface tension measurement according to

$$u_B = \frac{\Delta}{\sqrt{3}} \tag{3}$$

The relative uncertainties $\widetilde{u}_B$ were derived to

$$\widetilde{u}_B = \frac{u_B}{value} \tag{4}$$

The total relative uncertainty of one measurement was given to

$$\widetilde{u}_{B,tot} = \sqrt{\sum u_B^2} \tag{5}$$

For the keyhole measurements, equation (2) contains the parameters and assumed deviations Δ given in Table 1.

The values of the lowest keyhole section needed to be neglected for the evaluation, since the keyhole bottom alters the pressure conditions, and the simple assumption of a cylindrical element is not valid. Furthermore, the calculation considers the balance between the recoil pressure and the surface tension pressure, while hydrodynamic, hydrostatic pressure and the outflow of vapor was not considered due to their minor contribution to the pressure balance. Therefore, the calculated surface tension values below boiling temperature were neglected for the evaluation. The low temperatures of those elements rather indicate an unstable keyhole section.

4. Results

Surface tension values were derived at high temperatures of steel material using the derivation of surface tension values from the pressure balance in keyholes during laser treatment. At increasing laser intensity absorbed in a keyhole element, the capillary wall temperatures show an increasing tendency in the calculations, while the capillary widths show a slight decrease at increasing temperatures. In turn, the surface tension values must increase at increasing temperature. Since the calculation of surface tension values is based on the pressure balance between surface

Table 1
Assumed symmetrical deviations for the parameters in equation (2) including varying parameters.

Parameter	Value	Deviation Δ	Ref./origin
Keyhole radius r in mm	measured	±0.001	Pixel resolution
Intensity Iv in W/cm^2	calculated (ray tracing)	±1.00E+07	Ray tracing and sectioning resolution
Latent heat of vaporization Lv in kJ/kg	6580	–	[31]
Thermal diffusivity k in m/s^2	6.0E-06	±2.3E-07	[28] (at 1000 °C)
Molar gas constant R in J/(mol*K)	8.314471	±0.000014	[29]
Molar mass M in g/mol	55.845	±0.0005	[30]
Keyhole temperature Ts in K	calculated (ray tracing)	±10	Measuring deviation

tension pressure and the vapor pressure in the capillary element, the surface tension values calculated at temperatures below boiling are not valid, since the outflowing vapor and ambient pressure was not considered, which play a significant role in those regimes.

Above boiling temperature, surface tension values increase (Fig. 3).

5. Discussion

It was possible to develop a method to measure surface tension values indirectly from keyholes during laser irradiation. At higher pixel resolution in the X-ray imaging systems, the uncertainties can be decreased in the future. The temperature derivation is another source of uncertainty, which can be improved in the future using e.g. 3D models and a higher number of rays for a more precise energy input calculation in the keyholes. Although the measuring uncertainties are still quite high, tendencies are already visible.

In contrast to the expectations from linear extrapolations, an increasing tendency of surface tension values was seen (Fig. 3). Above boiling temperature, the observations of the keyhole sections in the X-ray images show the tendency of the keyhole sections to decrease in diameter at higher absorbed energy and temperature. According to the relation $p_{ST} = \sigma/r$ with the surface tension pressure p_{ST}, the surface tension coefficient σ and the radius r, a decreasing keyhole diameter/radius must be balanced by a higher surface tension to counteract the recoil pressure induced by the vaporization of the capillary walls. Otherwise, the vapor channel would expand as typically assumed when a higher recoil pressure occurs. This means that the decreasing tendency of the surface tension is changed into an increase at very high temperatures. Possible explanations of the increasing trend of surface tension values above boiling temperature can be suspected to be 1) the altered surface topology induced by atom losses due to vaporization of the surface layers and 2) the strength and kind of bonding forces between the surface atoms.

6. Conclusion

Using the keyhole system in high intense laser irradiation systems, it is possible to indirectly derive surface tension values at high temperatures of steel above boiling temperature. An increasing tendency of surface tension values above boiling temperature was observed. In the laser-induced keyhole, the sections that absorb most energy show highest induced recoil pressures, which should expand the keyhole section. However, since the keyhole sections show rather small diameters, the surface tension must increase to counteract the increased recoil pressure at the same time.

CRediT authorship contribution statement

Joerg Volpp: Writing – original draft, Visualization, Validation, Supervision, Project administration, Methodology, Investigation, Funding acquisition, Formal analysis, Conceptualization. **Yuji Sato:** Writing – review & editing, Data curation. **Masahiro Tsukamoto:** Writing – review & editing. **Lewin Rathmann:** Writing – review & editing, Data curation. **Marius Möller:** Writing – review & editing, Data curation. **Samuel J. Clark:** Writing – review & editing, Data curation. **Kamel Fezzaa:** Writing – review & editing, Data curation. **Tim Radel:** Writing – review & editing, Data curation. **Kevin Klingbeil:** Writing – review & editing, Data curation.

Declaration of competing interest

The authors declare that they have no known competing financial interests or personal relationships that could have appeared to influence the work reported in this paper.

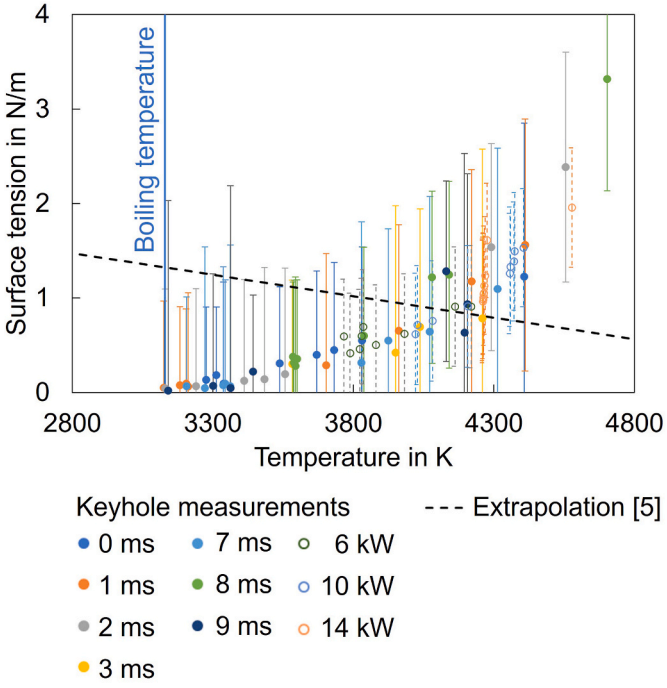

Fig. 3. Surface tension measurements above boiling temperature of steel including extrapolation from equation (1), while keyhole measurements of micro-welding at Argonne were done at varying time steps from 0 ms to 9 ms (laser wavelength 1070 nm, continuous wave, 200 µm spot diameter on the material surface, laser power 200 W at 200 mm/s process speed) and different laser powers during macro-welding in Osaka (laser wavelength 1070 nm, continuous wave, 350 µm spot diameter on the material surface at 6 m/min processing speed).

Data availability

Data will be made available on request.

Acknowledgements

The authors kindly acknowledge the funding of SMART – Surface tension of Metals Above vapoRization Temperature (Vetenskapsrådet - The Swedish Research Council, 2020–04250).

This research used resources of the Advanced Photon Source, a U.S. Department of Energy (DOE) Office of Science user facility operated for the DOE Office of Science by Argonne National Laboratory under Contract No. DE-AC02-06CH11357.

Special thanks go to the Patrick Faue, Brodan Richter, Mahmudul Hassan and Frank E. Pfefferkorn from the Department of Mechanical Engineering, University of Wisconsin-Madison, Madison, WI, 53706 USA, for the provision of the X-ray videos made at Argonne Laboratory.

References

[1] A. Marchand, J.H. Weijs, J.H. Snoeijer, B. Andreotti, Why is surface tension a force parallel to the interface? Am. J. Phys. 79 (10) (2011) 999–1008.
[2] A.S. Skapski, The surface tension of liquid metals, J. Chem. Phys. 16 (4) (1948) 389–393.
[3] B.J. Keene, Review of data for the surface tension of pure metals, Int. Mater. Rev. 38 (4) (1993) 157–192.
[4] G. Wille, F. Millot, J.C. Rifflet, Thermophysical properties of containerless liquid iron up to 2500 K, Int. J. Thermophys. 23 (5) (2002) 1197–1206.
[5] K. Morohoshi, M. Uchikoshi, M. Isshiki, H. Fukuyama, Surface tension of liquid iron as functions of oxygen activity and temperature, ISIJ Int. 51 (10) (2011) 1580–1586.
[6] V. Klapczynski, D. Le Maux, M. Courtois, E. Bertrand, P. Paillard, Surface tension measurements of liquid pure iron and 304L stainless steel under different gas mixtures, J. Mol. Liq. (2022) 118558.

[7] D.A. Padmavathi, Potential energy curves & material properties, Mater. Sci. Appl. 2 (2) (2011) 97–104.
[8] K. Tang, P. Kawka, R. Buckius, Geometric optics applied to rough surfaces coated with an absorbing thin film", J. Thermophys. Heat Tran. 13 (2) (1999) 169–176.
[9] P. Schott, N. de Beaucoudrey, C. Bourlier, Reflectivity of one-dimensional rough surfaces using the ray tracing technique with multiple reflections, in: International Geoscience and Remote Sensing Symposium, 7, 2003, pp. 4214–4216.
[10] H. Tostmann, E. DiMasi, P.S. Pershan, B.M. Ocko, O.G. Shpyrko, M. Deutsch, Surface structure of liquid metals and the effect of capillary waves: X-ray studies on liquid indium, Phys. Rev. B 59 (2) (1999) 783.
[11] C.J. Knight, Theoretical modeling of rapid surface vaporization with back pressure, AIAA J. 17 (5) (1979) 519–523.
[12] J. Drelich, C. Fang, C.L. White, Measurement of interfacial tension in fluid-fluid systems, Encyclopedia of surf. colloid sci. 3 (2002) 3158–3163.
[13] E.H. Trinh, P.L. Marston, J.L. Robey, Acoustic measurement of the surface tension of levitated drops, J. Colloid Interface Sci. 124 (1) (1988) 95–103.
[14] I. Egry, G. Lohoefer, G. Jacobs, Surface tension of liquid metals: results from measurements on ground and in space, Phys. Rev. Lett. 75 (22) (1995) 4043.
[15] K. Fahimi, L. Mädler, N. Ellendt, Measurement of surface tension with free-falling oscillating molten metal droplets: a numerical and experimental investigation, Exp. Fluid 64 (7) (2023) 133.
[16] S. Ozawa, S. Suzuki, T. Hibiya, H. Fukuyama, Influence of oxygen partial pressure on surface tension and its temperature coefficient of molten iron, J. Appl. Phys. 109 (1) (2011) 014902.
[17] V. Klapczynski, D. Le Maux, M. Courtois, E. Bertrand, P. Paillard, Surface tension measurements of liquid pure iron and 304L stainless steel under different gas mixtures, J. Mol. Liq. (2022) 118558.
[18] T. Leitner, O. Klemmer, G. Pottlacher, Bestimmung der temperaturabhängigen Oberflächenspannung des Eisen-Nickel-Systems mittels elektromagnetischer Levitation, TM - Tech. Mess. 84 (12) (2017) 787–796.
[19] V. Kolevzon, Temperature dependence of surface tension and capillary waves at liquid metal surfaces, J. Exp. Theor. Phys. 87 (1998) 1105–1109.
[20] A. Shmyrov, A. Mizev, A. Shmyrova, I. Mizeva, Capillary wave method: an alternative approach to wave excitation and to wave profile reconstruction, Phys. Fluids 31 (1) (2019) 012101.
[21] D. Nikolić, L. Nešić, Determination of surface tension coefficient of liquids by diffraction of light on capillary waves, Eur. J. Phys. 33 (6) (2012) 1677.
[22] Y. Minami, Surface tension measurement of liquid metal with inelastic light-scattering spectroscopy of a thermally excited capillary wave, Appl. Phys. B 117 (2014) 969–972.
[23] T.D. Bennett, C.P. Grigoropoulos, D.J. Krajnovich, Near-threshold laser sputtering of gold, J. Appl. Phys. 77 (2) (1995) 849–864.
[24] L. Shen, F. Denner, N. Morgan, B. van Wachem, D. Dini, Capillary waves with surface viscosity, J. Fluid Mech. 847 (2018) 644–663.
[25] J. Volpp, F. Vollertsen, Keyhole stability during laser welding—part I: modeling and evaluation, J. Inst. Eng. Prod. 10 (4) (2016) 443–457.
[26] J. Kroos, U. Gratzke, M. Vicanek, G. Simon, Dynamic behaviour of the keyhole in laser welding, J. Phys. D Appl. Phys. 26 (3) (1993) 481.
[27] J. Volpp, F. Vollertsen, Keyhole stability during laser welding—part I: modeling and evaluation, J. Inst. Eng. Prod. 10 (4) (2016) 443–457.
[28] H.P. Ebert, S. Braxmeier, D. Neubert, Intercomparison of thermophysical property measurements on iron and steels, Int. J. Thermophys. 40 (2019) 1–18.
[29] M.R. Moldover, J.P.M. Trusler, T.J. Edwards, J.B. Mehl, R.S. Davis, Measurement of the universal gas constant R using a spherical acoustic resonator, 1988 Mar-Apr, J. Res. Natl. Bur. Stand. 93 (2) (1977) 85–144, https://doi.org/10.6028/jres.093.010. Epub 1988 Apr 1. PMCID: PMC5179197.
[30] M.E. Wieser, T.B. Coplen, Atomic weights of the elements 2009 (IUPAC technical report), Pure Appl. Chem. 83 (2) (2010) 359–396.
[31] T.A. Sipkens, P.J. Hadwin, S.J. Grauer, K.J. Daun, Predicting the heat of vaporization of iron at high temperatures using time-resolved laser-induced incandescence and Bayesian model selection, J. Appl. Phys. 123 (9) (2018).